

GT2011-46336

**COMPUTATIONAL AND EXPERIMENTAL ANALYSIS OF AN INDUSTRIAL GAS
TURBINE COMPRESSOR**

Alexander Wiedermann
MAN Diesel & Turbo
Oberhausen, Germany
Member ASME

Ulrich Orth
MAN Diesel & Turbo
Oberhausen, Germany
Member ASME

Dirk Frank
MAN Diesel & Turbo
Oberhausen, Germany

Markus Beukenberg
MAN Diesel & Turbo
Oberhausen, Germany

ABSTRACT

Test rig results and their comparison with computational analyses of a highly-loaded 11-stage compressor for a newly developed industrial gas turbine will be presented in this paper. The scope of the tests has been validation of aerodynamic and mechanical features of the bladed flow path to meet both the demands for single- and dual-shaft operation of the gas turbine.

The test was carried out in three phases using extensive instrumentation. In phase 1 the front stages have been tested, and in phase 2 the test of the full 11-stage compressor was performed including numerous aerodynamic and structural check-outs. Vane and blade vibration modes were measured in all rows with numerous strain gauges using a telemetry system and Tip Timing, which additionally was applied to the front stage rotors. Concerning the mechanical design, finite element predictions of the vibration modes of all blades and vanes were carried out in the design phase to guarantee safe and resonance-free operation for a wide range of operational speeds which could be verified by the test data up to higher modes. Flow field computations were carried out with both a through flow solver and full 3-D viscous multistage solver based on Denton's TBLOCK, where all rotor and stator flow fields had been solved simultaneously and compared with experiments. The effects of tip clearance and stator cavities on compressor performance have been taken into account by the computational analysis. Effects of inlet distortion were examined in phase 3.

Comprehensive comparisons of computed and measured results will be presented. The extensive instrumentation gave also insight into flow details as vane pressure distributions and total pressure profiles in span wise direction. It will be shown

that the agreements of predicted and measured data were excellent.

INTRODUCTION

MAN performed the testing of a newly designed high performance axial compressor based on up-to-date high technology for its new industrial gas turbine in the range of 6-9 MW (1). The test rig compressor is a slightly scaled version of the gas turbine compressor and is designed for a pressure ratio of 14.6:1 with 11-stages and a design mass flux of 25.4 kg/s (rig size). Front rotor tip speed amounts 370m/s at the design point and the relative Mach number at the tip is slightly above one. It has been designed and tested for both two-shaft and single-shaft versions for the new gas turbine with application as single and combined cycle engines for mechanical drive operation and power generation. For the two-shaft engine application the rotational speed of the compressor can be varied between 75% and 105% of design speed to cover a wide range demanded by the mechanical drive operation. To cover the wide speed range the compressor is equipped with a variable inlet guide vane (IGV) and three additional adjustable stator vanes of the stages 1-3. For the mechanical design resonance free blade behavior has to be verified to allow continuous operation at any speed within this range. In preparation to the test extensive efforts to predict strength, vibration modes and aerodynamics have been done at MAN and later compared with the test data. The rig test was carried out at the test facility of Anecom AEROTEST at Wildau, Germany, which allowed full load operation for all requested operating points with the slightly scaled-down test compressor. Details on instrumentation, test execution and evaluation of the test data will be presented.

TEST COMPRESSOR AND INSTRUMENTATION

The purpose of the compressor test was the validation of the structural behavior and the aerodynamics of the blading. Unlike the construction of the gas turbine compressor, rotor disks have been replaced by a solid rotor design for simplicity and lower costs, Figs. 1 and 2. For easy installation in the test bed an axial intake was preferred instead of the more complex radial-axial inlet casing common for industrial gas turbines. This allowed us to investigate the compressor flow field performance in the first step. Inlet distortions due to the actual intake design of the gas turbine compressor were simulated by a bump in the inlet region which was optimized by CFD such that the distorted flow field at the inlet of the IGV represents the effect of radial- axial turning in the gas turbine intake.



Fig. 1: MAN test rig compressor

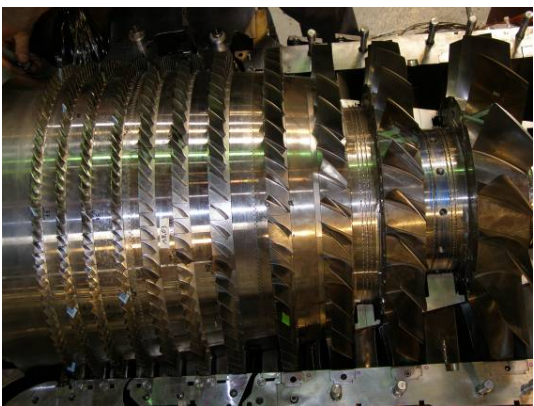


Fig. 2: Solid rotor built of MAN test compressor with rotor blade strain gauges

Instrumentation covered numerous pressure and temperature probes for aerodynamic performance data, strain gauges and telemetry system for vibration analysis, tip clearance and transient Kulite probes at selected blade rows. An overview of the test rig performance instrumentation for the full 11-stage compressor is shown in Table 1.

	Number of	Positions
Total pressure in the Intake	17	settling chamber
Total temperature in the Intake	4	settling chamber
Static pressure (Casing)	140 in total	Casing and diffuser wall
Dynamic pressure (Casing)	19 in total	R1(3), R2, R3, R4, R5, R7, R9, R10, R11 semi-infinite applications for R5 R11
Number of leading edge-temperatures	104 in total	S1(2x8), S2(2x8), S3(2x5), S4(2x5), S5(2x5), S6(1x4, 2x3), S7(3x3), S8(3x3), S9(2x3), S10(2x2), S11(2x2)
Number of leading edge-pressures	see leading edge temperatures	see leading edge temperatures
Number of measurement rakes (total pressure)	2 rakes with 5 heads 6 rakes with 3 heads	2 * at inlet (5) 6 * at compressor discharge / diffuser inlet (3)
Number of measurement rakes (total temperature)	2 rakes with 3 heads	2 * at compressor discharge / diffuser inlet (3)
Tip clearance measurement	5 stages with 4 probes	R1, R4, R5, R8, R11
Pressure distribution in mean section of guide vanes	5 stages with 7 holes on 2 vanes 35 in total	VIGV, S1, S2, S3, S7: 4 holes suction side, 3 holes pressure side
Number of strain gauges at guide vanes and rakes	49	stator surfaces
Number of rotating strain gauges	76	rotor surfaces
Mass flow measurement	Venturi (Main mass flow) orifices (in Bleed-ducts and buffer gas supply line)	
Power measurement	Torquemeter	
Engine speed measurement	Tooth wheel	
Blade Tip Timing	3 stages with 8 probes	2 LE, 2 TE of R1, R2, R3
Health and Safety Instrumentation in Bearing surroundings	10 pressures and 13 temperatures as necessary	front and rear bearing, oil supply, balance air cavity
Casing temperatures	30	Over R1, R5, R7, R11 close to annulus and close to outer wall in 3 circumferential positions
IGV angle measurement	16	VIGV, S1, S2, S3 4 Resolvers per stage, S7 mechanical indicator

Table 1: Test rig performance instrumentation

TEST PHASES AND PREPARATION

Overview

The compressor test was executed in 3 phases:

Phase 1: Only the transonic front stages were considered. At this stage of the test the aerodynamic performance was examined and the stability limits of the front stages confirmed. Blade strength data and vibration modes were taken for all rotors with strain gauges and a telemetry system. The distribution of the strain gauges was selected such that higher order modes as e.g. U, W – modes etc. could be resolved. In addition Tip Timing was applied to rotors 1 to 3 to monitor modes up to higher order for each individual blade of the front rotor rows. Aerodynamic data acquisition covers casing wall static pressure, leading edge total pressure and temperature and static pressure distributions along suction and pressure sides of selected stator vanes, see Table 1.

Phase 2: Test of the full 11-stage compressor was carried out. The instrumentation was extended to the middle and rear stages. As blade vibration modes had been obtained during the 5-stage compressor test, most of the strain gauges of the front rotors were removed in particular near the tip region which is

beneficial for the performance because the blockage due to probes and wiring is fairly high. The rear stage rotors and stators were fully instrumented to detect all the modes up to higher order which might be critical for the compressor.

Phase 3: After completion of the test of the blading performance in Phase 2 with ideal axial inflow the effect of inlet distortion was examined on both compressor performance data as well as on blade vibration amplitudes.

Aerodynamic analysis tools

Prior to the rig test, characteristics and flow field calculations had been performed with several codes. The first one is the mean line solver AXIAL, which has been upgraded and validated for multi-stage compressor design and analysis (2). This code is very efficient for concept studies, and calculation of compressor speed lines down to 20% of nominal speed is possible. Based on the results of AXIAL the compressor operating lines for the test had been determined. The characteristics within the design range had been calculated by a through flow solver ACFLOW which is based on the solution of the stream line equation with a finite element scheme. Extensive validation had been performed during the development phase of this code to obtain a universal tool valid for a wide range of application (3). This flow solver was extensively used for VGV-law optimization during the test.

In addition 3-D viscous computations were carried out with a customized version of the multi-block Navier-Stokes solver TBLOCK, which had been originally developed and extensively validated for turbine flow analysis by Denton (4,5). The code had been networked with MAN’s design and analysis environment (6) and calibrated for axial compressor flow analysis. Using a parallelized version allowed to solve all blade rows of the 11-stage compressor simultaneously with about 5-6 million grid points in total, distributed on 9 processors. An example of the flow field for front stages is shown in Fig. 3.

Because of its multi-block structured mesh topology it was possible to include the stator shroud geometries in the analysis and obtain insight into the effect of the clearance effects for the IGV and the first two stator vane rows which are shrouded whereas all other stators are of cantilever type. Fig. 4 shows the outline of the front stages, and typical results of the relative Mach numbers in the cavities are shown in Fig. 5. For simplification the number of seal fins was reduced to one in the numerical analysis, because we wanted to assess the global effect of the side wall cavities on the main flow instead to investigate details of the local flow pattern in the cavity region. For stator 1 and stator 2 the entire cavity flow domain could be covered in the stationary reference frame of the stators whereas in the cavity region of the IGV a mixing plane was necessary near the rotor 1 leading edge that it had to be included in the relative reference frame of the rotor.

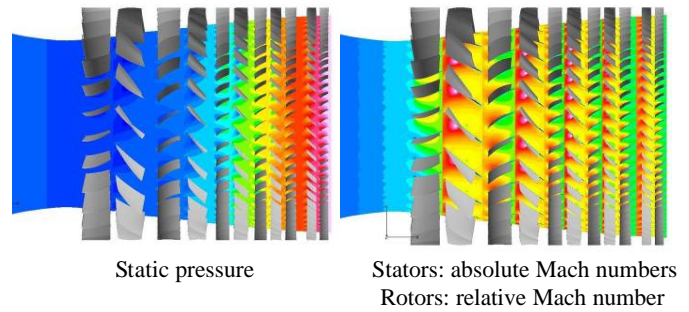


Fig. 3: Computed static pressure and Mach number distributions at mid span for the front stages

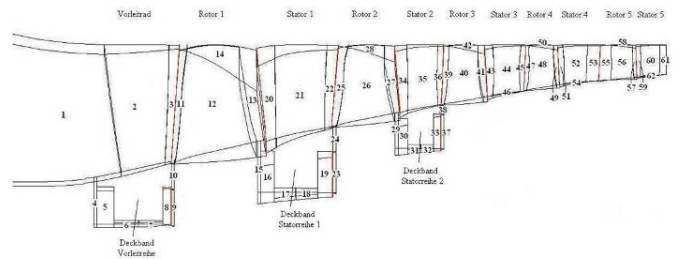


Fig. 4: Outline of computational domain including shroud and cavity geometry details for CFD- analysis

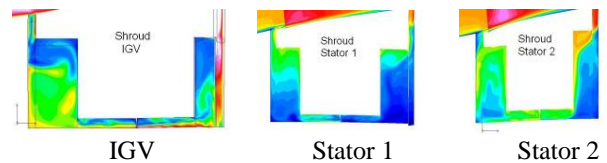


Fig. 5: CFD-results of relative Mach numbers in the cavity regions of IGV, Stator 1 and 2

Vibratory stress evaluation of blades and vanes

During the design process, the blade and vanes were laid out to satisfy their steady state and dynamic strength requirements. Both material temperature and stress level are key to the steady state operating strength of the blades and vanes which must sustain gas bending and centrifugal forces. Low Cycle Fatigue (LCF) caused by starting and stopping of the machine and High Cycle Fatigue (HCF) caused by flow disturbances are both critical in the strength evaluation of the blades and vanes. During compressor operation, the blades and vanes experience vibratory excitation at their natural frequencies by means of aerodynamic forces which are at frequencies which are multiples of the compressor’s running speed. For the described compressor test, the determination of actual blade and vane dynamic operating loads and thus the stress levels is of special importance. Knowledge of these loads leads to reliable operation of the compressor throughout a broad operating speed range.

In preparation for the operating test, the natural frequencies and mode shapes of all blades and vanes were determined by calculation and experimental means. Prediction of the blade and vane natural frequencies was performed using the finite element (FE) method. This method allows the frequencies to be calculated with and without the effects of temperature and centrifugal force. Therefore, the calculations can be compared to the bench test laboratory results and the measurements made during operation. The laboratory test determines the room temperature – zero speed frequencies using holographic methods. The individual blade or vane is held in specifically designed attachment blocks and preloaded to a defined load within the block. The holding block is attached to a piezoelectric mechanism to allow the blade or vane to be excited at its natural frequency. Two lasers are used to measure the displacements of the airfoil’s leading edge (LE) and trailing edge (TE) tips. The experimental set-up can be seen in Fig. 6 below. Fig. 7 shows typical LE and TE Tip displacements of a rotor blade being excited at various frequencies.



Fig. 6: Laboratory test set-up for natural frequency and mode shape determination

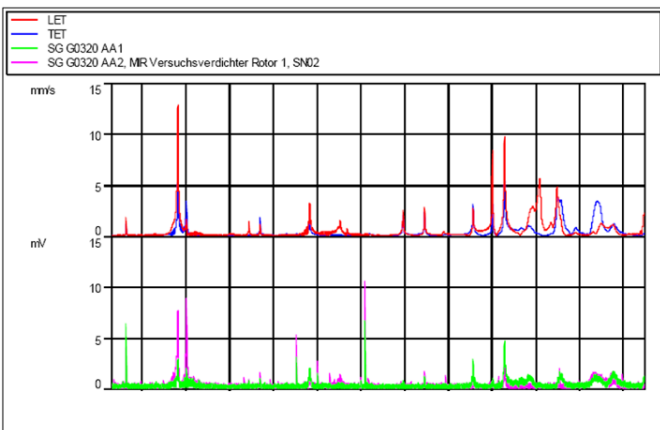


Fig. 7: Typical LE and TE displacement measurements during varying frequency excitation of a rotor blade

Calculated and measured mode shapes for a typical rotor blade are presented in the following Fig. 8. Comparisons for all blades and vanes show good correlation between measured and calculated values.

During operating tests, the blade and vane natural frequencies are excited by varying the compressor’s operating speed to correspond to their natural frequencies. To measure the true operating vibratory loads sustained by the blades and vanes, they were instrumented with multiple strain gauges. Specific gauge locations are chosen to aid in identifying each particular mode shape. To assure useful measured values each gauge needs to measure at least 40% of the maximum strain expected anywhere on the airfoil.

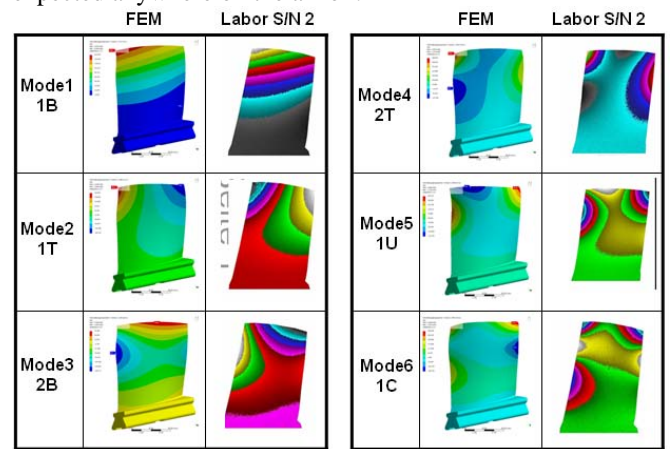


Fig. 8: Comparison between measured and calculated mode shapes for a rotor blade.

The measured strain at each strain gauge location must be correlated to the maximum strain within the airfoil for each mode shape. This is done through a table listing each gauge’s strain value as a percentage of the maximum strain experienced by the airfoil for each specific mode shape.

In the following Fig. 9, typical strain gauge locations A1 and A2 are shown. The gauges are radially oriented to detect bending and torsional mode shapes.

The signals from the gauges on the rotating rotor are transmitted to the stationary measuring devices by a telemetry system. Up to 20 different strain gauge signals can be processed at the same time. This allows for safe monitored operation of the test compressor throughout the planned operating speed range.

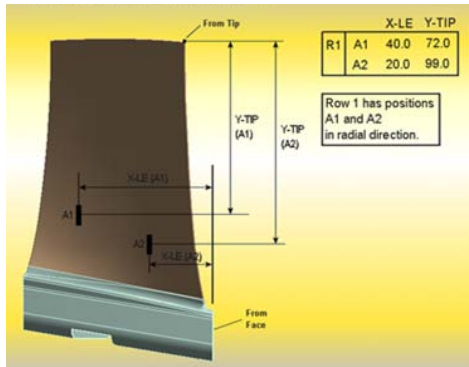


Fig. 9: Typical strain gauge locations on a rotor blade

The precise placement of the strain gauges is critical for all stages but especially for the back stages. Therefore, each instrumented blade and vane was laboratory tested to establish the percentage of maximum table previously predicted by FE calculation. Very good correlation between calculated and measured strains was observed for the lower mode shapes. For the higher modes, a broader scatter was observed.

The measured strain amplitudes, during the compressor test are directly compared to the blades resistance to HCF by use of a Goodman Diagram. It is essential to know the manufactured stated endurance limit of the airfoil. To establish the true endurance limit of each stage, individual blades were laboratory tested at specific frequencies and mode shapes. By incrementally increasing the excitation force and observing for crack initiation, the endurance limit of the airfoil is to be determined. Fig. 10 shows an example of a typical HCF test documentation.

Blade : R1		S/N: 19		Part No.: Maboko			
Temperature: RT °C							
Shaker	El-Dyn	No.:	LDS 826	Trimmass	mm O x mm		
Amplifier	PA 1000	Transmitter	None				
Frequency Generator	B&K	Typ:	B&K 1050	S/N:	ZZZ		
Air Jet Rig	None	Nozzle No.					
Torque Load							
Root / Holding Block:	4x 15	Nm	Shrout / HB:		Nm		
Holding Block / Shaker:	30	Nm	Mass/Shaker		Nm		
Amplitude Measure	GEVA 02	Microscope	0.1/10	mm	Resolution		
Calibration grid	Cal 0.1mm		S/N:		2		
Amplitude at:	LE Tip						
Fail at:	latter				8.0E+05 Cycles		
Mode 1	Mode 2	Mode 3	Mode 4	Mode 5	Mode 6	Mode 7	Mode 8
1F	1T	2F	2T	1C	-	-	-
Start (1)	Time	Runtime	"axf" LE	"axf" TE	Frequency	Amplitude	Remarks
Stop (0)	Std : Min	Std : Min	[mHz]	[mHz]	[Hz]	mm LE mm TE	
1	09:06		0.20		577.04	0.70	
	09:16		0.20		577.04	0.70	
	09:27		0.20		577.04	0.70	
	09:38	00:32	0.40		575.08	1.40	
	09:50		0.40		575.08	1.40	
	10:01		0.40		575.08	1.40	
	10:11	00:33	0.60		572.10	2.10	
	10:21		0.60		570.88	2.10	

Fig. 10: Example HCF-Test documentation

In addition to strain gauge measurements, the first three rotating stages were instrumented with a Tip Timing System

that measures the blade tip movements as a result of blade vibration. The system measures the LE and TE blade tip displacements in the tangential direction by optical sensors installed in the compressor casing on axial planes directly over the blade row. Up to eight sensors per row detect the relative displacement of the tips. The system processes this displacement information to determine vibration frequency and amplitude of the various blade mode shapes as they vary with rotor speed excitation sources. Fig. 11 shows the Tip Timing measurement data from one of the first stages for the first bending mode of the blades.

The strain gauge and Tip Timing measurements match very well. Since the Tip Timing system can measure every blade in the row, the maximum response of any blade can be identified and used to assure safe operation of the compressor.

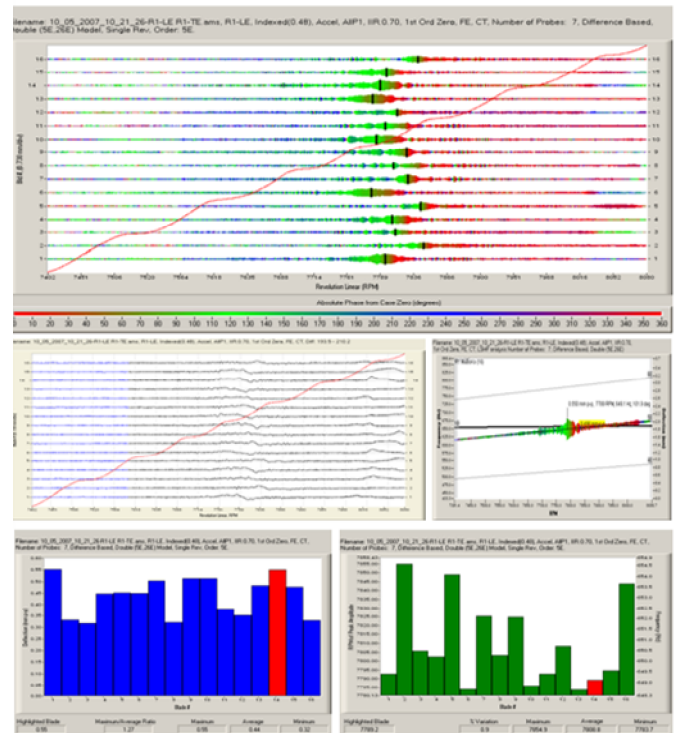


Fig. 11: Tip Timing Measurement Results for a Rotor Blade

TEST RESULTS AND DISCUSSIONS

Phase 1: 5-stage front stage rig test

Performance and operational range strongly depend on the quality of design and matching of the front stages. Therefore, only the front stages have been tested in the first phase of the test. The main objective of these investigations is to confirm and optimize the adjustment law for the IGV and the 3 VGV's Stator 1 – 3 and to determine sufficient stability limits of the front stages. Blade vibration modes of interest and amplitudes were examined. In this important component test it is possible

to analyze the front blade and vane strengths for rough off-design conditions including surge cycles.

Performance maps were taken for the nominal operating conditions, i.e. VGV vane adjustment at varied compressor speed, speed characteristics for VGVs held at design condition, and constant speed with varying VGV-settings. Characteristics of the front stages are shown in Fig. 12. All experimental data displayed are reduced to ISO condition at inlet ($T_{ref} = 288.15$ K, $p_{ref}=101325$ Pa). To avoid unfavorable decrease of gas turbine power at high ambient temperatures, the VGVs were held fixed at design settings in the range from 100% to 94.4% corrected speed (corresponding with a compressor inlet temperature of 50°C). For the remaining speed lines the VGVs were adjusted according to a linear actuation law. The switch between the two VGV adjustment laws can be clearly seen in Fig. 12 where a steeper slope of the surge line and reduced stability margin around the 94.4% - speed line can be observed.

The compressor inlet pressure could be reduced by a throttle ahead of the intake of the test compressor in order to reduce power and the mechanical blade loads at critical operating points. At the beginning of the test the inlet pressure had been throttled down to values between 50% and 80% of the ambient pressure depending on the operating condition, and mechanical as well as aerodynamic data have been taken at these inlet conditions. After the evaluation of the strain gauge results the compressor was run without inlet throttling except the operating points near the expected surge line. To obtain the stability margin of the front stages the test compressor was run into controlled surge at speeds of 80%, 94.4% and 100% respectively.

In the characteristics shown all measured data were corrected following (7) to compensate Reynolds number effects, and the coefficients of the correction formula were estimated by correlating all experimental data taken with various inlet pressures.

Ahead of the rig test, performance and stability ranges had been predicted by mean line [AXIAL, (2)], through flow [ACFLOW, (3)] and 3-D Navier Stokes [TBLOCK, (4)] analyses. In general, the agreement of computed results with experiments is very encouraging in particular in the vicinity of the design speed. 3-D CFD tends to overpredict the compressor capacity for low speed cases. All codes have in common that they underpredict the range of stable operation of the front stage arrangement which was measured at a considerably higher level than expected. It should be mentioned that blockage effects caused by the instrumentation on the measured results were not taken into account in the numerical analyses. In particular, the strain gauges applied near the OD of the rotors may have a considerable effect on the blockage which could explain the differences between measured and computed mass flows.

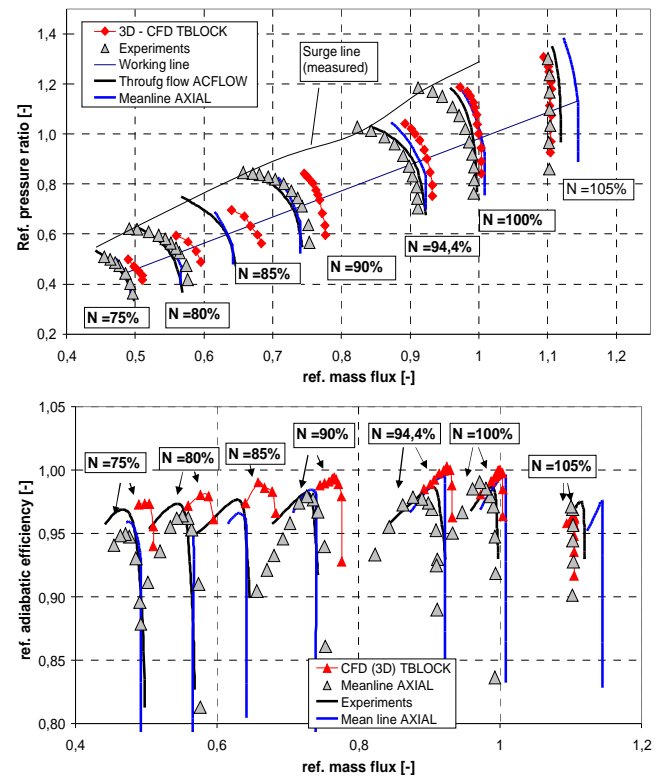


Fig. 12: **5-stage component test.** Comparison of experiments (Re-corrected) and predicted results. IGV, S1 – S3 were adjusted based on reduced speed except for the range of 94.4% and 100% speed

For the application of TBLOCK tip clearance flow was modeled using a gridded block for all rotors and cantilever stator blade rows. To quantify the effect of the leakage flow of the shrouded IGV, Stator 1 and 2, the cavities and seal fins have been modeled and compared for various gap heights. The purpose of this analysis was the investigation of the effect of the leakage flow on the blade row performance. Therefore, only one shroud seal fin was assumed. In our study we compared the solutions of the flow field for the case without shroud regions taken into account, and three different widths of the sealing gap with (1) nominal, (2) double, and (3) triple clearance. For the latter cases, pressure contours are shown in Fig. 13.

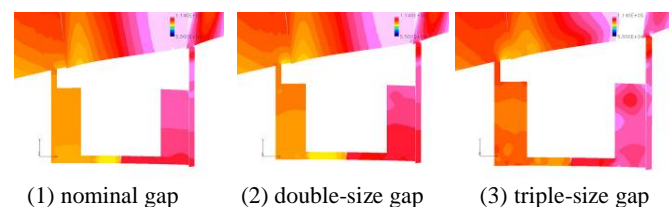


Fig. 13: Pressure distribution in shroud region of Stator 1 at three different clearances

The results demonstrate that duplicating the clearance does not have a strong effect on the pressure field whereas the pressure drop across the sealing fin is considerably affected if the clearance amounts three times of the nominal value. Comparisons of predicted characteristics show that the results with enlarged clearance mainly affect the stability limits for the critical hot day running condition. However the computed results with nominal gap width do not strongly deviate from the results for the case where the shroud effects have not been taken into account at all, Fig. 14. Therefore, for the analyses of the 11-stage compressor these blocks were omitted for the IGv and the two front stators in favor of reduced computational effort.

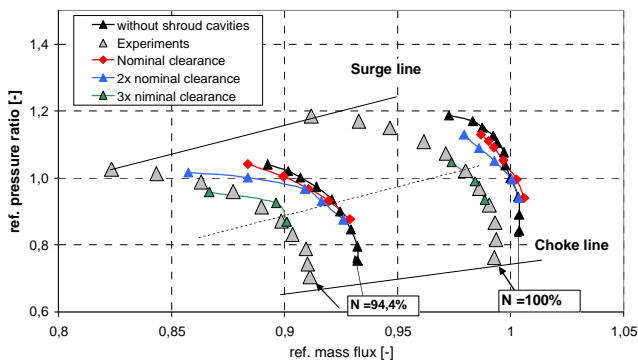


Fig. 14: Effect of IGv, S1, S2 – stator shroud flows on compressor performance

Phase 2: Full 11-stage compressor rig test

The test rig compressor is a modular design where the rear stages could be straightforwardly added to the rig using the identical hardware of the 5-stage compressor rig. The full 11-stage compressor had been equipped with two bleed ports where one is located behind stage 4 which is mainly used to start the compressor and to maintain a high level of stability margin below 85% speed. The meaning of the second bleed port at stage 8 is to simulate the extraction of a certain amount of cooling flow necessary for the turbine cooling flow system. During this test phase the effect of varying bleed flows was examined.

Strain gauges were applied to rotors and vanes of stages 6 – 11 to cover all critical vibration modes. To reduce blockage most of the strain gauges of rotors 1 – 5 were removed for this test phase except at the rotor base where the bending stresses should be monitored during surge cycles. Rotors 1 to 3 were monitored using Tip Timing.

The compressor characteristic is shown in Fig. 15. In this case the VGv's were adjusted for each speed line according to a similar law as used for the 5-stage compressor rig test. Though the compressor test facility driver engine at Anecom AEROTEST allows full-load operation of the compressor for

all operating points, most data have been taken with inlet throttling to reduce power and to protect the compressor at critical off-design operating conditions as those near choke and stall. To obtain the stability limit of the compressor it was run into controlled surge at 80% and 100% speeds. In these cases the compressor could be recovered quickly, and blade stress levels observed during the surge cycles were moderate. All experimental data shown are corrected based on Reynolds number (7).

The agreement of measured and predicted data is good for all steady-state operating points considered. Adiabatic efficiencies are overpredicted by AXIAL. It is remarkable that the agreement of predicted and measured surge limit is very good with all solvers, in particular around the design speed.

Compared to the results of the 5-stage rig test, Fig. 12, the agreement between measured and computed mass flux is considerably better which may be due to the fact that for the full stage test the strain gauges at the outer diameters of the rotors were removed. This observation underscores the assumption that blockage effects of OD instrumentation have a strong impact on measured mass flux.

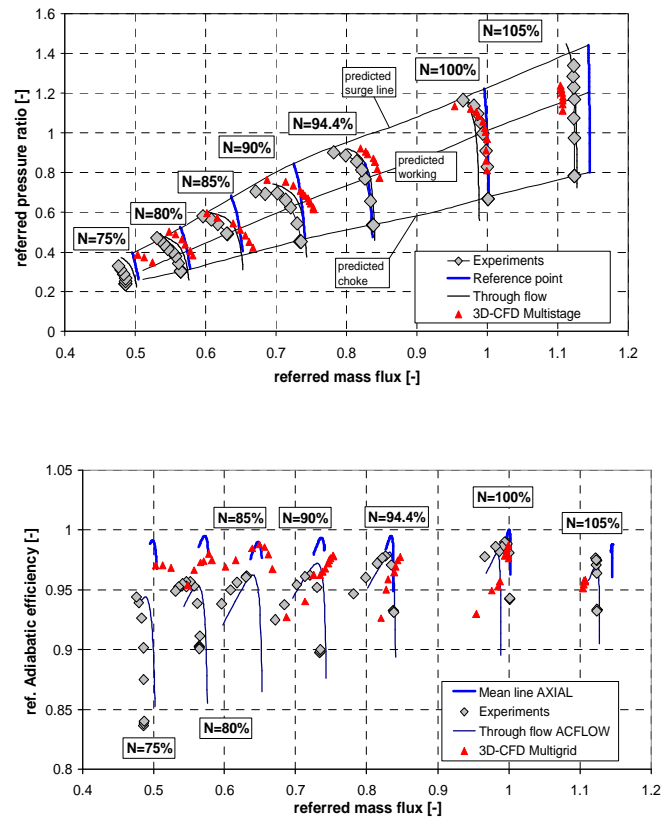


Fig. 15: 11-stage component test. Comparison of experiments (Re-corrected) and predicted results. IGv, S1 – S3 were adjusted dependent on reduced speed

Fig. 16 shows an excellent agreement of measured and predicted pressure rise within the compressor as given by the results of the static pressure probes along the casing.

Details of the inter stage flow fields were obtained with total pressure and temperature probes mounted at the leading edges of selected vanes in all stages. Depending on the blade height up to 8 probes could be applied. In the rear stages the measured data were taken at 5 span wise stations, where the probes had to be distributed to two representative vanes as only 3 probes could be mounted along the tight leading edge. An example of an instrumented vane is shown in Fig. 17.

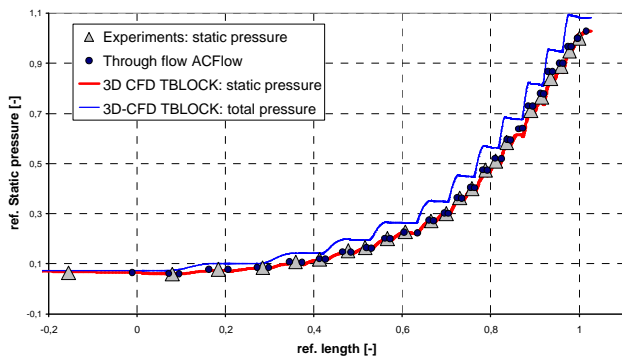


Fig. 16: Comparison of casing static pressure probe measurements with predicted results



Fig. 17: Variable Stator 3 leading edge total pressure probes

Fig. 18 shows span wise distributions of total pressure and temperature and predicted mean averaged values with ACFLOW and TBLOCK at the stator leading edge planes of each stage for the design point. The comparison of the slopes suggests a reasonably good agreement of prediction and experiments. 3-D CFD gives a more pronounced boundary layer like structure near the side walls. It should be mentioned that the results of TBLOCK and ACFLOW have been obtained prior to the testing, and no attempt was made to fit the correlations of ACFLOW to the test results.

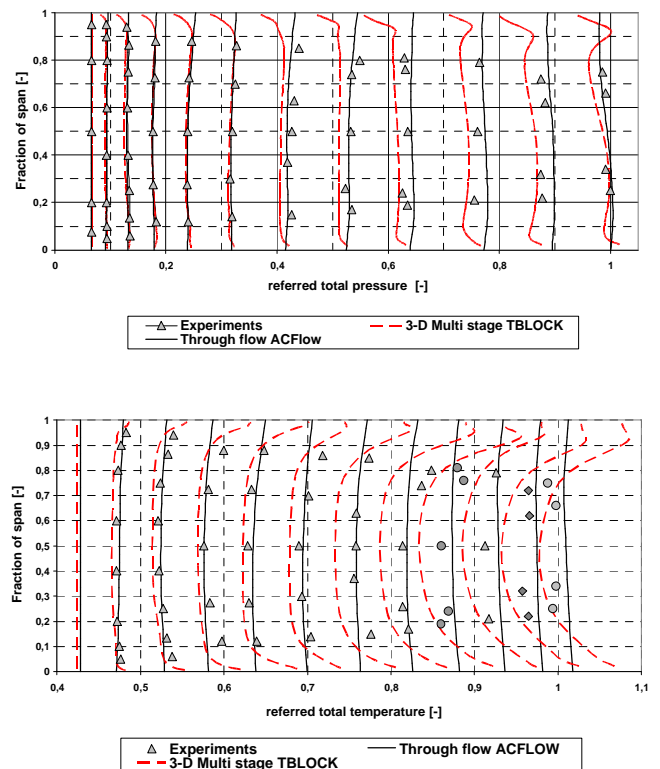


Fig. 18: **11-stage compressor test:** Comparison of measured and predicted total pressure and temperature distributions. 100% speed, design pressure ratio

More details about the flow at the blades were obtained with mid span static pressure measurements along the suction and pressure sides of selected vanes of the IGV, stators 1 to 4 and stator 7 rows. A comparison of measured and predicted distributions is shown in Fig. 19 which offers much insight in pressure levels and incidences.

Experimental values of the stage pressure ratios were obtained using the area-averaged results of the leading edge probes. This information offers details about the loading of the individual stages and their stability margins. The results for all stages can be combined in a single graph when the mass fluxes are reduced to ISO conditions using the averaged total pressure and temperature at the leading edge plane of the stators. Results for the design speed ($N=100\%$) are shown in Fig. 20 covering the entire operating range from choke to surge. Overall the match between measured and predicted results is reasonably good. Deviations observed for stages 2, 3 and 4 could be explained by uncertainties inherent with measurements of total pressures and temperatures using leading edge instrumentation.

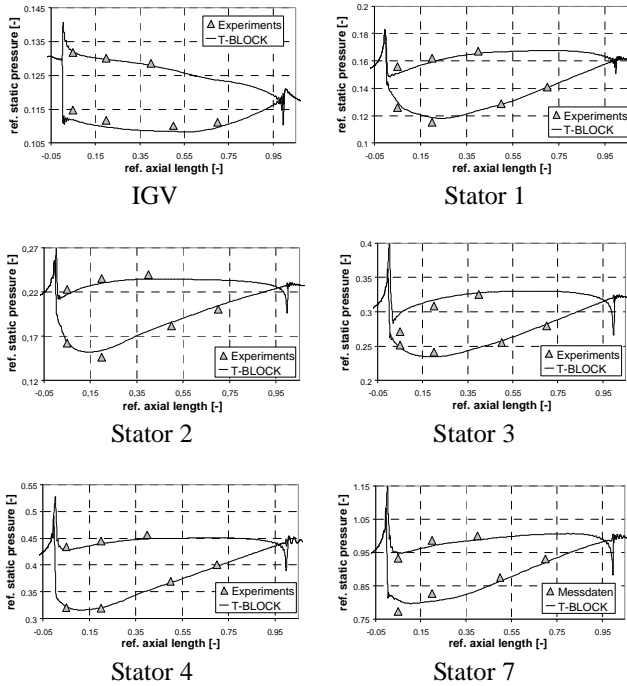


Fig. 19: **11-stage compressor test:** Comparison of measured mid span pressures with 3-D CFD (TBLOCK). $N=100\%$ speed, design pressure ratio.

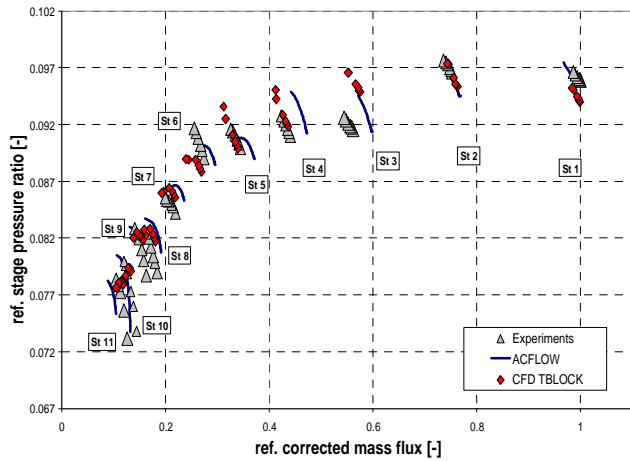


Fig. 20: **11-stage compressor test:** Measured and predicted stage pressure ratios. $N=100\%$ speed (stage pressure ratios are referred to the total pressure ratio)

VGV- Optimization: As mentioned above it is desirable to reduce the drop in power when the gas turbine is operated at higher inlet temperatures. To achieve this goal it is favorable to operate the gas turbine compressor at design setting of the VGV within a wide temperature range, i.e. corrected speed. During the 5-stage compressor rig test (phase 1) it was found

that safe operation of the front stages could be achieved at 94.4% corrected speed (corresponds with 50°C ambient temperature). On the other hand the slope of the surge line becomes steeper in this region, and the stability margin decreases. During the test of the 11-stage compressor the optimum setting has to be carefully looked for by VGV-optimization studies. It is well known that operation at more open VGV settings means that the front stages are most highly loaded, and, therefore, it is useful to consider the stability margin of the front stage group of the compressor.

The procedure of this optimization can be best explained by comparing the pressure ratio results of the 5-stage compressor test with those of the front stages obtained with the measured data of the leading edge probes, Fig. 21.

Looking at the operating line of the front stages of Fig. 21 it is obvious that it is shifted towards higher pressure ratios at the 11-stage compressor operation condition (see orange line). With the original VGV-law the front stage group of the compressor would have sufficient stability margin with regard to the surge line of the 5-stage compressor rig (see orange symbols). The green symbols indicate the hot day results of the front stage group if the VGV-stagger angles are fixed at their design setting (100% speed), and indicate rather tight stability margin for this condition.

VGV-optimization was executed with the aim at finding more favorable flow condition at hot day operation. As already mentioned the stagger angles of the IGV and the three adjustable front stators could be actuated individually. Among all variations an optimum setting could be found, indicated by blue symbols in Fig. 21, where the mass flux could be raised by 4% without compromising the efficiency. With this setting the stability margin of the 11-stage compressor could exceed the design target value for all conditions.

It must be mentioned here that in principle stable operation is achievable with open VGV at hot day condition for single-shaft gas turbine operation. However, dual-shaft gas turbines operated over a wide speed range demand for higher stability margins at all operating speeds because of more frequent transients inherent with mechanical drive operation.

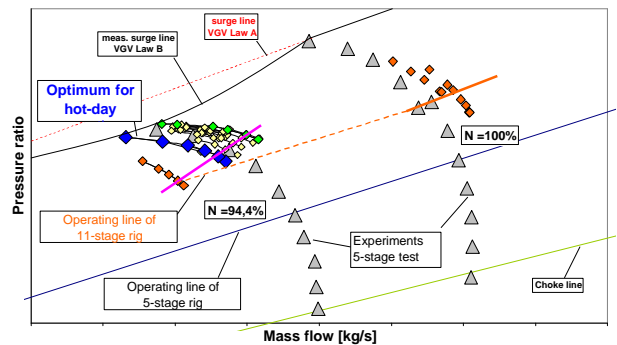


Fig. 21: **11-stage compressor rig test:** Optimization of VGV-setting for hot day running condition ($T_{amb} = 50^\circ\text{C}$)

Constant speed characteristics: The compressor is designed for both dual-shaft and single-shaft operation, and for several application requirements it must be proven that the compressor mass flux can be safely controlled at constant speed by adjusting the variable guide vanes. The corresponding characteristics are shown in Fig. 22. With regard to the design setting the IGV was adjusted in the range from -10° (open) to $+30^\circ$ (closed), and S1 – S3 were following a corresponding sequence. It could be verified that for all operating conditions the blade stress levels do not exceed critical values. Again, predicted results are close to the experiments.

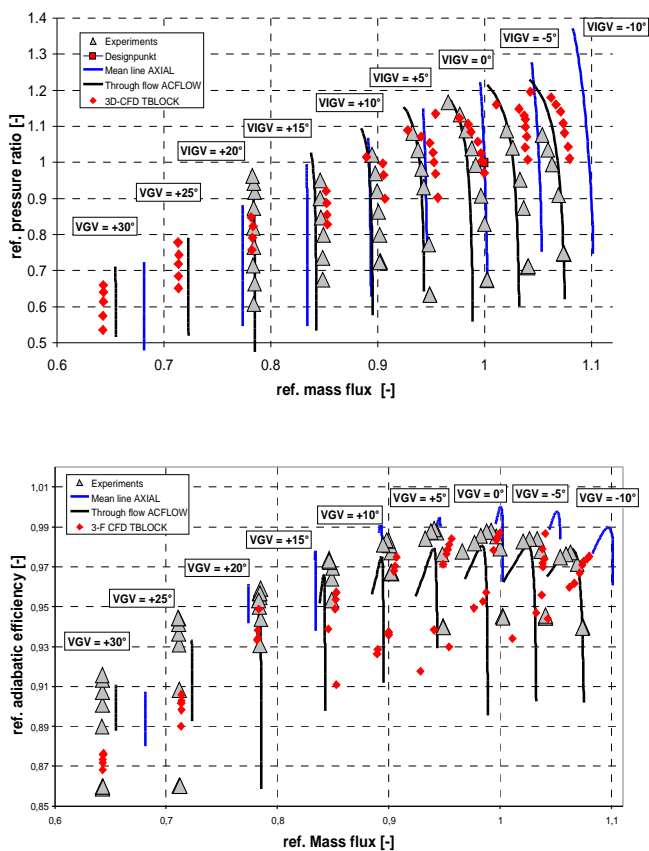


Fig. 22: **11-stage compressor test.** Comparison of experiments (Re-corrected) and predicted results. 100% speed ISO, variable VGV setting

Phase 3: Inlet distortion

In contrast with the gas turbine built, where the inlet casing turns the flow from radial into axial direction, all tests were carried out with an ideal axial intake to examine the compressor blading performance. However, inlet distortion can have strong impact on compressor performance and stability.

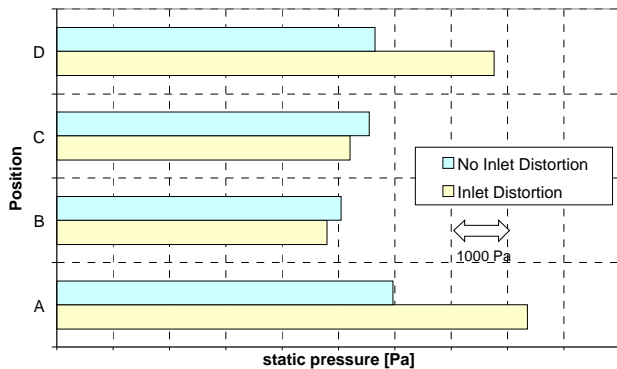
Very often, the dimensions of inlet casings are restricted by rotor dynamics constraints. An CFD-based inlet casing was designed following the well-known DC60 criterion (8,9). Extensive numerical steady-state and unsteady analyses have been performed to judge interaction effects of the inlet casing and the transonic front rotor of this compressor (10). To validate the procedure, it was decided to investigate the effect of inlet distortion during the compressor rig test.

For this purpose a bump has been designed for the inlet duct to simulate the effect of the radial-axial turning inlet duct of the gas turbine, Fig. 23. The surface shape was determined using CFD, and its structure could be easily mounted in the rig intake. Its length, curvature, thickness and mounting location was determined to simulate the flow features downstream of a 90 degree turning gas turbine intake as best as possible without producing undesirable separation zones and stream wise vortex pattern.

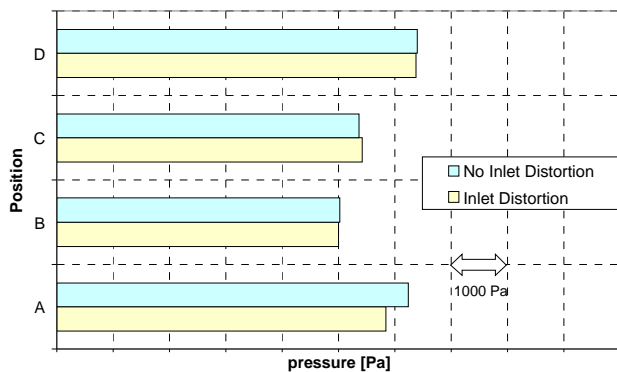


Fig. 23: Bump to simulate inlet distortion

Compressor characteristics were taken for the 100%, 94.4% and 90% speed lines up to the stability limit. As predictions show (10), almost no effect on 11-stage compressor performance and stress levels could be observed. The reason for this can be found when looking at the static pressure variations in circumferential direction which were taken in front of and behind the IGV vane row at 4 lateral locations, Fig. 24. Just in front of the IGV, the distortion of the pressure field could be clearly seen. However, the non-uniformities have virtually disappeared after the flow has passed through the IGV vane row. This means that the presence of the IGV has a filter effect to eliminate non-uniformities which were generated downstream of the compressor.



(a) In front of IGV



(b) Behind IGV

Fig. 24: Effect of simulated inlet distortion on circumferential pressure distribution in front of and behind the IGV vane row

CONCLUSIONS

Execution and results of several rig tests of components of a gas turbine compressor have been described which covered a separate test of the front stages, the full 11-stage compressor rig test and the effect of inlet distortion. Prior to the test, predictions of the compressor characteristics had been performed with the mean-line flow solver AXIAL, the through-flow solver ACFLOW and the Navier-Stokes solver TBLOCK. The design target could be achieved, and the compressor proved to be safe and efficient for all the operation scenarios of a gas turbine compressor. Good agreement of experiment and theory demonstrates a high standard of the design and analysis tools used. With regard to inlet distortion the compressor was shown to be insensitive because of the filter effect of the IGV which almost deletes lateral non-uniformities in the flow field. In summary, the new compressor fulfills all requirements of the operating conditions of the new gas turbine in 6-9 MW range.

ACKNOWLEDGMENTS

This work was supported by publicly funding technology programmes "Rationale Energieverwendung und Nutzung unerschöpflicher Energiequellen REN", contract 85.65.69-T-196, and "Regionale Wettbewerbsfähigkeit und Beschäftigung (EFRE)", contract 64.65.69 EN 1011A by the state of North-Rhine Westphalia, Germany, and "Ziel II Phase V" of the European Union. The authors wish to thank MAN Diesel & Turbo SE, Oberhausen, Germany for its support of this work and for granting permission to publish this paper.

REFERENCES

1. Beukenberg, M.; Wiedermann, A.; Orth, U.; Aschenbruck, E.; Reiß, F., 2010: The New 6MW Gas Turbine of MAN (in German). VDI-Report 2095, Stationäre Gasturbinen, Leverkusen, 2010, pp. 199-213.
2. Dubitsky, O.; Wiedermann, A.; Nakano, T.; Perera, J., 2003: The reduced Order Through-Flow Modeling of Axial Turbomachinery. Proc. Int. Gas Turbine Congress 2003 Tokyo, Paper TS-052.
3. Petrovic, M.; Wiedermann, A.; Banjac, M., 2009, Development and Validation of a New Universal Through Flow Method for Axial Compressors. ASME GT2009-59938.
4. Denton, J.D., 2005: Multiblock CFD – Solver TBLOCK", Cambridge University, UK
5. Rosic, B.; Denton, J.D.; Curtis, E.M., 2007: The Influence of Shroud and Cavity Geometry on Turbine Performance. ASME GT2007-27769 and -27770 (part 1 + 2)
6. Wiedermann, A., 2004: Industrial CFD-based Design System Development for Turbomachines. Newsletter of the ASME-Branch in Japan, Tokyo.
7. Wassell, A. R., 1968: Reynolds Number Effects in Axial Compressors. ASME Journal of Engineering for Power, April 1968, pp. 149 – 156.
8. Reid, C., 1969: The Response of Axial Flow Compressors to Intake Flow Distortion. ASME-Paper 69-GT-29.
9. Zierer, T.; Matyshok, B., 1997: Design, Development and Verification of Gas Turbine GT24 Air Intake. Proceedings of ASME Asia, Singapore.
10. Hilgert, M.; Böhle, M.; Cagna, M.; Wiedermann, A., 2011: Stationary Gas Turbine Intake Design and its Impact on a Transonic Compressor Stage. Prepared for the 9th European Conference on Turbomachinery (ETC), Istanbul.